Low-energy electron diffraction from Cu(111): Subthreshold effect and energy-dependent inner potential; surface relaxation and metric distances between spectra

S. Å. Lindgren and L. Walldén
Physics Department, Chalmers University of Technology, S-412 96 Göteborg, Sweden

J. Rundgren and P. Westrin
Department of Theoretical Physics, The Royal Institute of Technology, S-100 44 Stockholm, Sweden
(Received 28 February 1983; revised manuscript received 12 October 1983)

In the present low-energy electron-diffraction (LEED) study of the copper (111) surface the inner potential and the surface relaxation are determined independently from the subthreshold effect and from Bragg-type diffraction. A "subthreshold effect" is a narrow LEED intensity structure occurring at a setting where new beams have an emergence threshold in the metal: a "subthreshold." We reconsider the absorption of electrons with regard to its spatial distribution in the crystal and design a phenomenological model comprising two parameters which are adjusted to the absorptive scattering cross section of the ion cores and that of the interstitial region. The two-parameter model for the interlayer attenuation indicates the existence of a transparent scattering channel "pseudoparallel" to the surface for beams emerging in the crystal. The channeling extends over all layers penetrated by the LEED electrons, giving the subthreshold effect a peak width of about 2 eV. Each observable subthreshold effect fixes a point on the energy-dependent inner potential; for the copper (111) surface we are able to measure the inner potential at 19.5-, 73.6-, and 109-eV incidence energy. A local excited-state potential of the Hedin-Lundqvist type produces for the copper (111) surface an inner-potential curve that agrees well with the measured points. From LEED spectra for the 00, 10, and 01 beams from the copper (111) surface in the energy range 16—190 eV we infer a top-layer spacing contracted $(0.7\pm0.5)\%$ relative to the layer spacing in the bulk. The theoretical and experimental spectra are compared by means of metric distances, which are stable with respect to noise in the data and give a linear response to small variations of the structural parameters.

I. INTRODUCTION

We have observed that the specular low-energy electron-diffraction (LEED) spectrum from the (111) surface of copper contains narrow features which are poorly described by customary LEED theory. The narrow features are observed when the incidence of the primary beam is close to normal, and they occur near threshold energies where new beams start to propagate in the metal. We shall refer to narrow features associated with a beam threshold in the metal as the "subthreshold effect,"[1] using the prefix "sub" to make a distinction from the "threshold effect," or Rydberg fine structure,[2] connected with the grazing emergence of beams in the vacuum.

At very low energy and normal incidence where only the specular beam is reflected from the surface, a shoulder at 19.5 eV leaning against a Bragg peak at 22.5 eV attracts particular attention. The shoulder is the second most intense part of the entire specular spectrum and is correlated with the threshold at approximately 18 eV where six beams, those equivalent by symmetry to 10 and 01, are emergent in the metal. At higher energies and near-normal incidence similar structure is observed in the neighborhood of the sixfold degenerate 11 and 20 thresholds in the metal. Similar observations are made by Bedell and Farnsworth[3] on the copper (111), nickel (111), and cadmium sulfide (0001) surfaces, and by Jaklevic and Davis[4] on the (111) surfaces of six fcc metals.

An intriguing fact is that the subthreshold effects are considerably narrower than 2β, where β is the absorptive inner potential. To study the phenomenon we have reconsidered the absorption of electrons and its distribution in the ion cores and in the interstitial region. In a theoretical model where we assume the absorption to be lower in the ion cores than in the interstitial region, the interlayer flux transmitted by the beams emergent in the metal is reinforced in comparison with the situation that the absorption is uniform in the layer. These beams open an important scattering channel almost parallel (within 10°) to the surface. In all layers penetrated, the primary beam scatters a flux into the transparent channel, which in turn rescatters some flux into the specular beam. One finds that a scattering channel which is pseudoparallel to the surface and extends over many layers will create constructive interferences narrower than 2β in the visible beams.

Our LEED calculations on the copper (111) surface reproduce the observed subthreshold effect with excellent accuracy. Because its creation takes place in the bulk, the subthreshold effect proves insensitive to surface relaxation. An inference of great physical interest is that the narrow spectral features fix a number of points on the inner-potential—versus—energy curve $V_0(E)$.

In a recent LEED investigation, Tear *et al.*[5] have recorded 21 beam spectra in the energy interval 50—400 eV and fit theory to data whose center of gravity lies in a region where the inner potential is constant to a good approximation; they report $(0.3\pm1)\%$ contraction of the top-layer spacing. Using a much smaller data base, the 00, 10, and 01 spectra in the energy region 16—190 eV, we find the contraction $(0.7\pm0.5)\%$. We argue that the agreement with the previous elaborate investigation is not accidental but is due to our establishing, firstly, the energy-dependent inner potential from the subthreshold effect and, secondly, the top-layer spacing from the Bragg structure of the spectra. Extensive photoemission measurements show that the low-index surfaces of copper have a number of electronic surface bands below the Fermi level.[6–8] A good knowledge of the deformation of the lattice near the surface, such as the relaxation of the top-layer spacing, is a necessary prerequisite for surface-band calculations.

For the calculation of the inner potential, which is strongly energy dependent in the region 16—190 eV considered in this work, we use the Hedin-Lundqvist version local-density theory.[9] We have treated the potential part of the LEED calculations in two earlier papers[10,11] and found that the local-density theory gives excellent agreement with LEED experiments when applied to aluminum[10] and copper.[11]

The comparison of theoretical and experimental LEED intensities is made in a novel manner by means of metric distances between beam spectra and sets of beam spectra.[12] The search for a new measure of the misfit between theory and experiment was started in the course of this work since it was felt that current reliability indexes,[13–15] based on the differentiation of data, depend too much on the curve-smoothing procedure. The calculation of the metric distances involves integration of spectra and is therefore stable with respect to noise in the data. The metric distances have the interesting property that they give a linear response to small variations of the structural parameters.

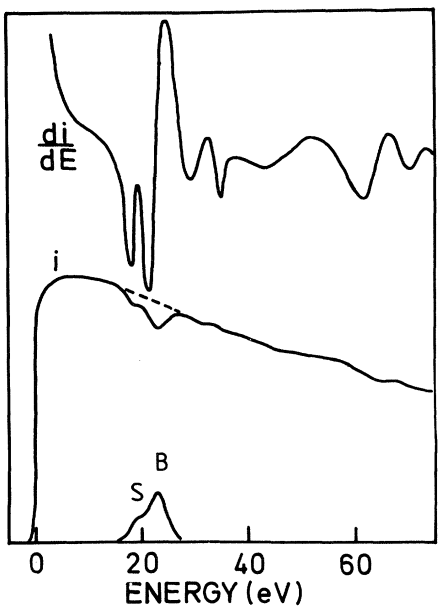

FIG. 1. Sample-to-ground current $i(E)$ in an experiment on LEED from the copper (111) surface. Normal incidence. Inset at the bottom shows the specularly reflected intensity. *B* denotes Bragg peak, and *S* denotes subthreshold effect. See Secs. III C and IV B.

The paper is organized as follows. In Sec. II the LEED experiment on the copper (111) surface is described, and particular attention is paid to the specular spectrum in which a strong and narrow feature is observed at very low energy. In Sec. III the layer-Korringa-Kohn-Rostoker (KKR) model for LEED is provided with an electron absorption distributed less on the ion cores and more on the interstitial region, opening a transparent scattering channel pseudoparallel to the surface and creating a subthreshold effect in the visible beams. In Sec. IV, LEED spectra are calculated and surface parameters are found which represent the experimental spectra with great accuracy both with respect to major peaks and subthreshold effects. In Sec. V metric distances between spectra are used for measuring the misfit between theory and experiment. In Sec. VI we establish that observed subthreshold effects fix the shape of the inner-potential—versus—energy curve $V_0(E)$, and we sum up the physical properties of metric distances between spectra.

II. EXPERIMENT

The LEED experiment was made with standard three-grid display optics and a spot photometer. A disk-shaped sample of 25 mm diam. and 1.5 mm thickness was spark-cut from a rod (delivered by Materials Research Corp.), and the (111) surface was oriented by spark erosion to within 1°. Before being mounted the sample was mechanically polished and electropolished as described by Tegart.[16] The sample was cleaned inside the vacuum chamber by cycles of argon-ion bombardment (1 μA, 250 eV) followed by heating (750 K). The temperature was measured by a thermocouple located in one of four spark-drilled holes used for fixing the sample to a molybdenum ribbon which served as a holder and a heater. A surface with a particularly high electron reflectivity was obtained if the sample was kept at an elevated temperature (650 K) during the final ion bombardment. The pressure was about 10^{-10} Torr.

One can observe the specular beam at normal incidence in a narrow energy range around 20 eV by bending the reflected beam out from the axis of the electron gun by means of a magnetic field and a small sample tilt. We first obtained evidence that this was an interesting observation to make by recording the sample to ground current as a function of the primary energy at normal incidence. As seen in Fig. 1, the current-versus-energy curve shows a dip on the low-energy side of the minimum at 22.5 eV above the vacuum level. The dip is very sensitive to the angle of incidence and is observed only within 2° from the surface normal. It can therefore be used to check that the electrons are incident near the normal direction after proper adjustment of the magnetic field. When the primary beam is set at normal incidence in the manner just described, it turns out that the intensity of the specular

beam is the inverse of the sample to ground current shown in Fig. 1. The 00 spectrum has a major peak at 22.5 eV, and, superposed on that, a shoulder at 19.5 eV. The major peak corresponds to a Bragg reflection at the (111) layers of copper.

In the present work beam intensities are normalized to unit incident current. The electron to photon efficiency of the fluorescent LEED screen is in good agreement with the sample-to-ground current curve in Fig. 1, which shows that the intensity of the Bragg peak at 22.5 eV is 10%. The measured LEED spectra for the 00, 10, and 01 beams are discussed together with calculated spectra in Sec. IV.

The observation of the shoulder at 19.5 eV in the 00 spectrum poses a straightforward theoretical problem. On one hand, the shoulder is the second largest structure in the beam spectra from the copper (111) surface next to the Bragg peak at 22.5 eV. On the other hand, the shoulder is hardly resolved at all by customary LEED calculations, which reproduce most other features of the measured spectra. We find that the shoulder at 19.5 eV depends on the distribution of the electron absorption on the ion cores and on the interstitial region.

III. A NEW MODEL FOR THE INTERLAYER ATTENUATION

A. Interlayer propagator

The absorption of LEED electrons in the crystal is described phenomenologically by means of an imaginary inner potential β which is energy dependent. The absorption enters at two stages in the LEED formalism: in the complex phase shifts describing the scattering within a single layer and in the propagators accounting for the phase change and attenuation between layers. The complex phase shifts result from a matching of the radial wave functions in the ion-core muffin-tin potential $V_{\mathrm{MT}}(r)+i\beta$ against attenuated plane waves in the interstitial region of potential $V_0+i\beta$. In the customary LEED formalism[17–20] the interlayer propagator P_g of beam $\vec{g}$ has the magnitude (in Rydberg atomic units)

$$|P_g| = \exp[-\mathrm{Im}(k_{gz})d] , \qquad k_{gz}=(E-V_0-|\vec{k}_{xy}+\vec{g}|^2-i\beta)^{1/2} , \tag{1}$$

where d is the interlayer spacing, E is the primary energy, V_0 is the real inner potential, and $\vec{k}_{xy}$ is the surface component of the wave vector $\vec{k}$ of the incident electron. The crystal is the half-space $z>0$. Expression (1) gives a first approximation to the interlayer attenuation, corresponding to a picture where the LEED electron is an attenuated plane wave in jellium of potential $V_0+i\beta$.

We now consider a physical picture where the absorptive potential is nonuniform in space, $\beta_{\mathrm{MT}}(E,\vec{r})$ in the muffin tins and $\beta_{\mathrm{IR}}(E,\vec{r})$ in the interstitial region. The corresponding probability densities of the LEED electron, $|\Psi_{\mathrm{MT}}(\vec{r})|^2$ and $|\Psi_{\mathrm{IR}}(\vec{r})|^2$, are, in general, different from a simple attenuated plane wave. The total absorption cross section of a unit cell of an atomic layer is[21]

$$\sigma_{\mathrm{abs}}(E)=\sigma_{\mathrm{abs,MT}}(E)+\sigma_{\mathrm{abs,IR}}(E) , \tag{2}$$

where

$$\sigma_{\mathrm{abs},i}=-\frac{1}{k}\int_i \beta_i(E,\vec{r})\,|\Psi_i(\vec{r})|^2 d^3r , \quad i=\mathrm{MT,IR} \tag{3}$$

corresponding to a distribution of sinks in the muffin tin (MT) and the interstitial region (IR). A first approximation for the interlayer attenuation is given by expression (1), which for a fixed energy E has a single parameter $\beta(E)$. This can be adjusted so as to give a correct value of $\sigma_{\mathrm{abs}}(E)$.

A second approximation of the interlayer attenuation is one in which the total absorptions $\sigma_{\mathrm{abs},i}(E)$, $i=\mathrm{MT,IR}$, are fitted separately. We shall propose a model where the ion cores are rolled out to a slab of uniform thickness as indicated in Fig. 2. The ion-core slab and the interstitial slab (consisting of two disconnected parts) have thicknesses pd and $(1-p)d$, where p is the packing fraction of the MT's in the crystal volume. Touching spheres have $p=0.74$ in a fcc crystal and 0.68 in a bcc crystal. In the jellium picture a beam $\vec{g}$ propagating in an absorbing material is a plane wave, $\exp[(i\,\mathrm{Re}(k_{gz})z]$, times an attenuation function, $\exp[(-\mathrm{Im}(k_{gz})z]$. We shall now take the attenuation to be $\exp[-\mathrm{Im}(k_{gz})(1-p)d]$ across the interstitial plate and $\exp[-\mathrm{Im}(k_{gz})p_{\mathrm{abs}}d]$ across the ionic plate, where p_{abs} is a new parameter. The condition that the interstitial plate has the total absorption $\sigma_{\mathrm{abs,IR}}(E)$ settles β, and, with β fixed, the condition that the ionic plate has the total absorption $\sigma_{\mathrm{abs,MT}}(E)$ determines p_{abs}. As a second approximation of the interlayer attenuation we therefore introduce the expression

$$|P_g| = \exp[-\mathrm{Im}(k_{gz})(1+p_{\mathrm{abs}}-p)d] . \tag{4}$$

The slab model is compatible with the surface periodicity of the crystal. Depending on whether $p_{\mathrm{abs}}<p$ or $p_{\mathrm{abs}}>p$, the ion-core slab is transparent or opaque, respectively, compared with the interstitial slab. Of the inelastic-scattering processes accompanying LEED, the plasmon excitation has the largest scattering cross section. The plasmons involve the valence electrons, which are kept away from the ion cores by the orthogonality of the electron orbitals. Since possible excitations of the ion cores, as in the Auger process, have very small cross sections at LEED energies, the ion-core slab is apt to be transparent. From a phenomenological determination of p_{abs} and β in the case of LEED by the copper (111) surface, we find $p_{\mathrm{abs}}=0.44$ as compared with $p=0.74$ (Sec. IV B).

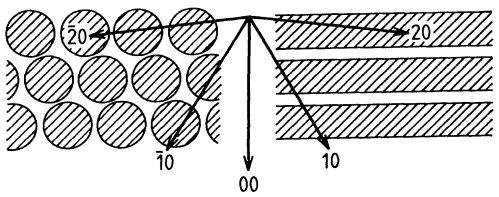

FIG. 2. Electron absorption in LEED: Ion cores are transparent and interstitial region is opaque, relatively speaking. MT model (left) and slab model (right). $\vec{k}$ vectors illustrate the channeling of subemergent beams.

The slab model for the regions of different absorption requires that the layers parallel to the surface are close packed, or almost so, and that the interlayer spacing is large. Possible instances are the low-index surfaces of fcc, bcc, and hcp crystals.

B. Emergence of beams in the crystal

The second approximation of the interlayer attenuation given by expression (4) is particularly interesting in connection with the emergence of a new beam in the crystal. Using a kinematical picture we shall say that the electron of a beam $\vec{g}$ carries the energy $E_{gz}=E-V_0-|\vec{k}_{xy}+\vec{g}|^2$ with its propagation normal to the surface, and we shall divide the beams inside the crystal into three kinds: (i) the propagating beams having $E_{gz}\gtrsim|\beta|$, (ii) the beams close to internal emergence where E_{gz} is in the interval $\pm|\beta|$, and (iii) the evanescent beams having $E_{gz}\lesssim-|\beta|$. The corresponding imaginary wave vector component is

$$\mathrm{Im}\,k_{gz}=\begin{cases}\frac{1}{2}E_{gz}^{-1/2}|\beta|\ , & E_{gz}\gtrsim\beta| \\ (\frac{1}{2}|\beta|)^{1/2}\ , & |E_{gz}|\lesssim|\beta| \\ |E_{gz}|^{1/2}, & E_{gz}\lesssim-|\beta|\ .\end{cases} \tag{5}$$

We normalize the interlayer attenuations $|P_g|$ of the beams $\vec{g}$ by setting $|P_0|$ equal to $\exp(-a_0 d)$, where a_0 is an attenuation exponent which can be determined from experimental data by means of a LEED calculation. In the new notation we have

$$\beta=-2a_0E_{0z}^{1/2}(1+p_{\mathrm{abs}}-p)^{-1} \tag{6}$$

and

$$|P_g|=\begin{cases}\exp(-a_0E_{0z}^{1/2}E_{gz}^{-1/2}d), & E_{gz}\gtrsim|\beta| \\ \exp[-a_0^{1/2}E_{0z}^{1/4}(1+p_{\mathrm{abs}}-p)^{1/2}d], & |E_{gz}|\lesssim|\beta| \\ \exp[-|E_{gz}|^{1/2}(1+p_{\mathrm{abs}}-p)d], & E_{gz}\lesssim-|\beta|\ .\end{cases} \tag{7}$$

The conclusions are (i) that the propagating beams are independent of p_{abs} to a very accurate approximation, (ii) that the beams about to emerge in the crystal have an attenuation exponent proportional to $(1+p_{\mathrm{abs}}-p)^{1/2}$, and (iii) that the evanescent beams rapidly become unimportant irrespective of p_{abs} when E_{gz} decreases below $-|\beta|$. As a consequence, the amplitude of the internally emergent beams becomes enhanced when p_{abs} is smaller than p. In such a case an important scattering channel is opened through the internally emergent beams.

Here a few words on terminology are appropriate. In the literature on LEED the notions "beam threshold," "grazing emergence," and "preemergent" are related to a beam $\vec{g}$ having an energy close to $E=|\vec{k}_{xy}+\vec{g}|^2$. It is possible experimentally to determine this energy to any desired accuracy by observation of the Rydberg resonances that are created by the reflection of beams in the image-potential barrier.[22] In the present paper we study the diffuse threshold of extension $E=|\vec{k}_{xy}+\vec{g}|^2+V_0\pm|\beta|$, where the beams in the crystal turn from the evanescent mode into the propagating mode. In order to distinguish one beam threshold from the other we refer to the low-lying diffuse threshold as the subthreshold, and to a beam gradually becoming propagating in the crystal as a subemergent beam. Narrow interference features created by excited subemergent beams and appearing in the spectra of the visible beams are referred to as a subthreshold effect.

C. Subthreshold effect

With a purpose of studying the subthreshold effect we suppose that the nth layer has the beam scattering matrix $M_{ngg'}^{ss'}$ where $\vec{g},\vec{g}'$ label the beams and s,s' (each being positive or negative) indicate their direction of propagation along the surface normal. The field of the LEED electrons in the metal is fed by the primary beam penetrating successively through the layers. In each layer the primary beam pumps an electron flux into all of the beams. In particular, a subemergent beam $\vec{g}$ receives a flux of amplitude $|M_{ng0}^{s+}||P_0|^n$ in the nth layer and transmits a flux of amplitude $|M_{ngg}^{ss'}||P_g|$ from one layer to the next. Another part of beam $\vec{g}$, $|M_{n0g}^{-s}||P_g|$, is scattered into the specularly reflected beam. The contributions collected by that beam in different layers n interfere, and if the beam $\vec{g}$ is excited so that $|P_g|$ is large, a subthreshold effect consisting of substantial interference fringes will be observed in the specular beam. The effect is enhanced at symmetry settings where several subemergent beams occur simultaneously.

From the above scattering scenario it is possible to estimate the least possible linewidth of a subthreshold effect. We consider the case that the primary energy is varied at a fixed direction of incidence. The fluxes pumped by the primary beam into a subemergent beam $\vec{g}$ at different layers below the surface are beating wavelets, in general, but occasionally the wavelets are in phase from one layer to the next. In such a case, they add up to a single wave having the wave vector $\mathrm{Re}k_{gz}=(|\beta|/2)^{1/2}$ and the same attenuation exponent a_0 as the primary beam. The wave $\exp[(i\mathrm{Re}k_{gz}-a_0)z]$ can be expressed as a superposition of stationary waves in $\vec{k}$ space,

$$\Psi_g=\int_0^\infty A(k)\exp(ikz)dk\ , \tag{8}$$

with a Breit-Wigner intensity distribution

$$|A(k)|=\{4\pi^2[(k-\mathrm{Re}k_{gz})^2+a_0^2]\}^{-1/2}\ . \tag{9}$$

Its full width at half maximum (FWHM) is $\Delta k = 2a_0$ and gives a peak of width $\Delta E = 2\,\mathrm{Re}k_{gz}\Delta k$ in the visible energy spectra. The estimated peak width is, from expression (6),

$$\Delta E = (8\,|\beta|\,)^{1/2}a_0 = 4a_0^{3/2}E_{0z}^{1/4}(1+p_{\mathrm{abs}}-p)^{-1/2}\,. \qquad (10)$$

The parameter a_0 can be estimated from a LEED calculation on the copper (111) surface at 100 eV where the penetration of 20 layers spaced 2.1 Å apart attenuates the beam intensities by a factor of the order of 10^{-3}. In the case considered, where $a_0 = 0.043$ a.u. and $\beta = -4.5$ eV ($p = 0.74$ and $p_{\mathrm{abs}} = 0.44$), one or more constructive interferences of linewidth $\Delta E = 1$ eV can appear in the visible beams in a 9-eV window enclosing a subthreshold. The observed width is about 2 eV.

A possible dependence of β on the $\vec{k}$ vector of the primary beam gives rise to corrections of the interlayer attenuations of the beams. The study made by Rasolt and Davis[23] seems to indicate that intensity variations due to the incident $\vec{k}$ are broad compared with the narrow features ensuing from p_{abs}.

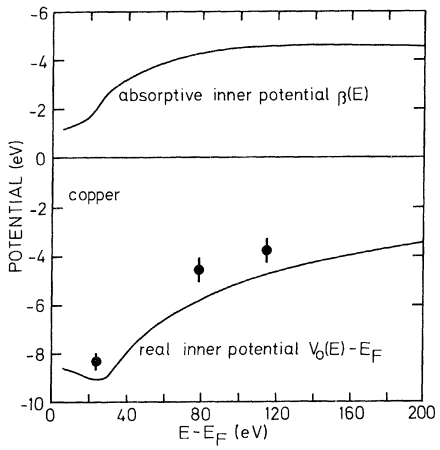

FIG. 3. Complex inner potential of copper $V_0(E)+i\beta(E)$ as a function of the primary electron energy E. $V_0(E)$ is theoretical (Refs. 9 and 11) and $\beta(E)$ is phenomenological (Ref. 11 and this work). Three V_0 values determined from the subthreshold effect are plotted.

IV. LEED CALCULATIONS ON THE COPPER (111) SURFACE

A. Computer program, crystal potential, and beam spectra

LEED calculations were made by means of a layer-KKR program.[18] In the cases where an experiment has normal incidence or an oblique incidence in a mirror plane of the crystal, the code utilizes crystal symmetry for reducing the plane-wave and angular momentum representations of the wave field. The symmetry routines are permanent in the program and are activated simply by the input of the symmetry elements of the two-dimensional (2D) space group of the crystal surface; the input follows the standards of *International Tables for X-ray Crystallography*.[24] The program takes up to 10 phase shifts, but eight phase shifts give sufficient accuracy for copper in the considered energy range, 16–190 eV. The interlayer scattering is calculated by the method of layer doubling,[17] and the scattering at the crystal face is simulated by the nonreflecting barrier or, as the case may be, by the image-potential barrier.[25]

The input of complex phase shifts is obtained from a crystal potential whose exchange-correlation part is a local excited-state potential of the type devised by Hedin and Lundqvist.[9] The design of a crystal potential for copper is described in two papers by Neve *et al.*[10,11] and the resulting energy-dependent inner potential $V_0(E)$ is illustrated in Fig. 3. In the same figure we show a phenomenological absorptive inner potential $\beta(E)$ which we have obtained by adjusting the calculated peak widths to the experimental ones. The diagram for β is used together with the value 0.44 for p_{abs}; further discussion about the choice of p_{abs} is contained in Sec. IV B. Furthermore, the calculated intensity depends on the termination of β in vacuum. Since the spill out of β only scales the heights of the peaks with their widths preserved, we take the liberty of cutting off β half an interlayer spacing outside the topmost layer. The work function is 4.8 eV; the Debye temperature is set at 343 K for the copper bulk[26] and 300 K for the top layer.

The intensity of the 00 beam was recorded with the surface normal of the sample tilted 5° away from the axis of the electron gun towards [10] in the reciprocal surface net. As a check we varied the incidence angle in the calculations and found that 5° off-normal incidence in fact gives the best fit to the experiment. The intensities of the 10 and 01 beams were measured and analyzed at normal incidence. The measured and calculated spectra are shown by diagrams in Figs. 4–6.

In order to facilitate visual inspection the calculated

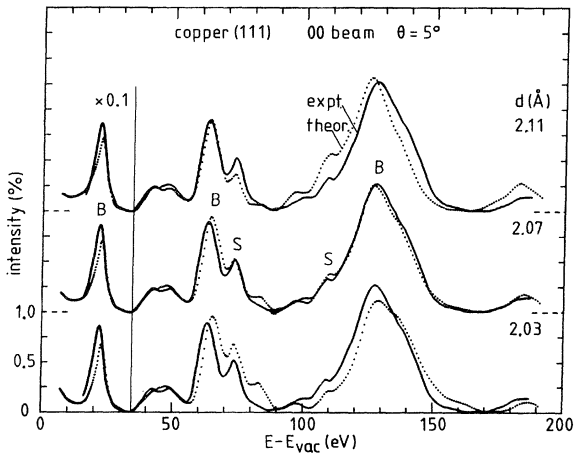

FIG. 4. 00 spectrum from the copper (111) surface at an incidence tilted 5° away from the normal towards [10] in the reciprocal surface net. LEED calculation uses the precalculated inner potential $V_0(E)$. Intensity scale is beam current relative to unit incident current in the experiment (the calculated spectrum is reduced by the factor 0.53). d is the interlayer spacing at the surface. B denotes Bragg peak and S denotes subthreshold effect.

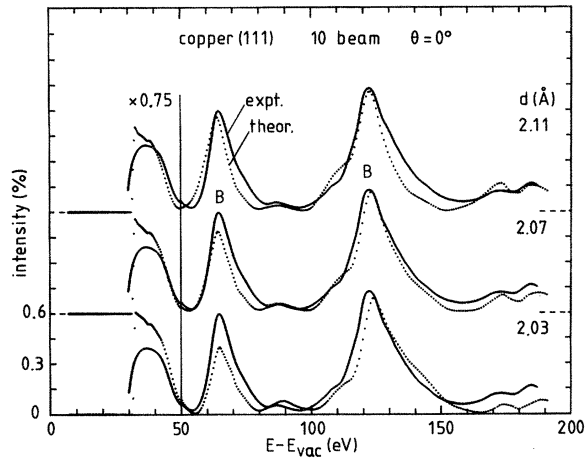

FIG. 5. 10 spectrum from the copper (111) surface at normal incidence. Same symbols as Fig. 4.

spectra are displayed on top of the measured ones; furthermore, a set of spectra is shown on either side of the best choice of surface relaxation. When the calculated 00, 10, and 01 intensities are scaled by a common factor, 0.53, they are brought into excellent agreement with the experimental ones. Letters *B* indicate Bragg reflections calculated kinematically and referred to the energy-dependent inner potential. The best agreement between theory and experiment is established by means of a misfit measure, called metric distance, described in Sec. V. The result is that the calculated inner potential $V_0(E)$ in Fig. 3 is lifted by a shift of the order of 1 eV, and we infer that the spacing between the two topmost atomic layers is contracted by $(0.7\pm0.5)\%$ relative to the interlayer spacing in the bulk.

The calculated and measured spectra in Figs. 4–6 agree well everywhere with the exception of the 01 spectrum in the range 85–105 eV, where the theory has two maxima

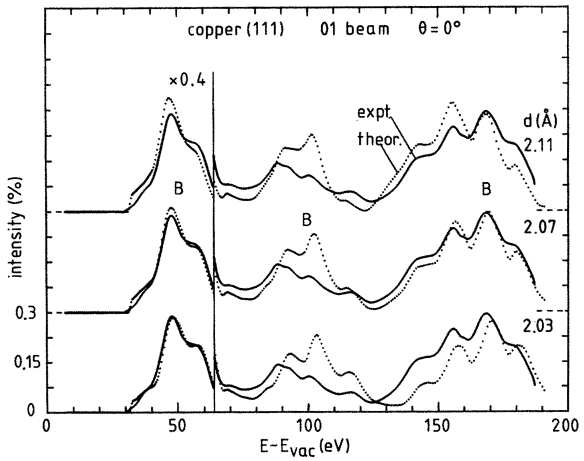

FIG. 6. 01 spectrum from the copper (111) surface at normal incidence. Same symbols as Fig. 4. Near 100 eV the 01 beam emerges in a direction where the differential cross section for the direct scattering from the primary beam has a node (Sec. IV A and Fig. 7).

which lie right in energy but have intensities which differ from the measured values. In this energy range it is observed experimentally that the intensity spectrum of the 01 beam is extraordinarily sensitive to the angle of incidence.

A kinematical study explains why the experiment and the calculation are particularly difficult in the energy range 85–105 eV. At 101 eV and normal incidence the 01 beam undergoes diffraction in directions corresponding to the scattering angle 148° relative to the direction of incidence. The differential scattering cross section of the ion core of copper $\sigma(\theta)$ has a minimum close to zero at $\theta=145°$, and when the primary energy varies over the range 85–105 eV the 01 beam scans the backscattering minimum of $\sigma(\theta)$. In Fig. 7, $\sigma(\theta)$ is shown by a Cartesian and a polar diagram. Although the beam intensities are amplified by Bragg reflection, the direct scattering from the primary beam to the 01 beam remains low; the multiple scattering through several scattering vectors is predominant and very sensitive to phases. In consequence, if the ion-core scattering differs the least from the ideal model, the calculated spectrum of the 01 beam in the (85–105)-eV range is expected to give poor agreement with the measurement.

B. Subthreshold effect and the inner potential

Figure 8 shows a series of LEED calculations where β and p_{abs} are adjusted simultaneously in such a manner that the intensity of the major peak at 22.5 eV is kept approximately equal to the measured value, 10% of the incident intensity. Multiplying the β curve in Fig. 3 by a coefficient $c=(1+p_{abs}-p)^{-1}$ as indicated by expression (6), we find, when a decrease of p_{abs} is balanced by an increase of $c\beta$, that a shoulder comes up and grows to a narrow peak. Since the experimental setup has a finite resolving power, the correct theoretical curve should exhibit a somewhat sharper structure than the recorded spectrum. The calculated structure accurately agrees with the measured one at 19.5 eV for $p_{abs}=0.44$, provided the calculated inner potential V_0 in Fig. 3, is lifted 0.7 eV.

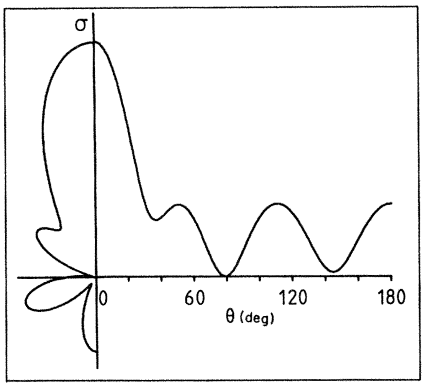

FIG. 7. Differential scattering cross section σ for the ion core of copper at 100 eV. Polar diagram (left) and Cartesian diagram (right); θ is the scattering angle. Scale is $\ln(1+\sigma)$, which is linear for σ small and logarithmic for σ large.

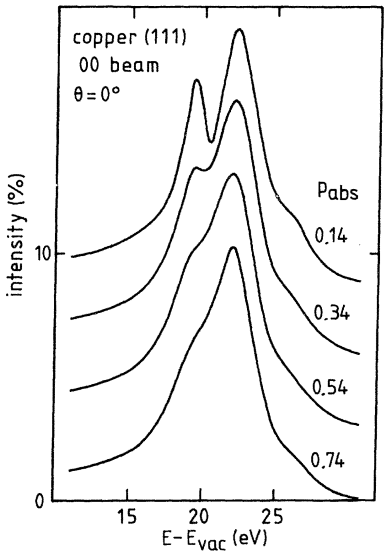

FIG. 8. Four calculations of the subthreshold effect at 19.5 eV in the specular LEED spectrum from the copper (111) surface at normal incidence. The value $p_{abs}=0.74$ corresponds to uniform absorption in a fcc crystal, and with decreasing p_{abs} the ion-core region becomes transparent; $p_{abs}=0.44$ agrees with the observed spectrum in Fig. 1.

We have made a series of tests by means of the LEED program to study the effect of the new parameter p_{abs}. Neither an image-potential barrier at the surface,[25] including possible variations of the parameters of that barrier, nor a relaxation of the topmost interlayer spacing has any effect on the narrow feature brought about by a low value of p_{abs}. The shoulder is thus explained by scattering in the bulk.

Our LEED program shows that the shoulder at 19.5 eV can, in fact, be produced in a calculation where $p_{abs}=p$ and $c\beta=0.7$ eV instead of the value $\beta=2.2$ eV in Fig. 3. However, under these circumstances the calculated intensities of the Bragg peak and the shoulder grow to unrealistic values, 30% and 15%, instead of the measured ones 10% and 5%. Recently, Jaklevic and Davis[4] calculated the reflectivity of the copper (111) surface for normal incidence in the range 16—26 eV using a band-structure scheme. With a 1-eV absorptive potential, a Bragg peak, and a shoulder of 35% and 20% intensity (the measured[4] shoulder is 5%) are obtained much in the same way as in the last-mentioned LEED calculation. It appears that the band structure interprets the shoulder at 19.5 eV in the 00 intensity from the copper (111) surface as a reflectivity enhancement due to symmetry selection and that the channeling concept considered in this work is needed to explain the measured intensities.

Having established the subthreshold effect at 19.5 eV in the 00 spectrum one is, in fact, able to localize other instances of the same effect at higher energies. In the reciprocal net the three innermost hexagons centered around the origin have angles at the points 10, 11, and 20, respectively. At normal incidence each one of the hexagons corresponds to six beams which have threshold in the vacuum at 30.8, 92.2, and 123.1 eV and in the metal near 17, 84, and 110 eV [these are *a priori* values obtained from $V_0(E)$ in Fig. 3]. In the present LEED experiment the crystal was tilted 5° from the normal when the 00 intensity was recorded. In that case, the sixfold-degenerate subthresholds at 84 and 110 eV become divided into several subthresholds in the energy regions 70—98 and 95—139 eV. The considered subthreshold effects in the 00 spectrum are listed in Table I. When studying the spectra in Fig. 4, one finds that the subthreshold effects are practically fixed on the energy scale irrespective of surface relaxation, whereas the coarse spectral features marked as Bragg peaks move quite substantially when the surface relaxation is varied.

In addition to the large subthreshold effect at 19.5 eV,

TABLE I. Subthreshold effects in the 00 spectrum from the copper (111) surface at or near normal incidence. $h\,k$ denotes subemergent beams, and θ is the angle of incidence with respect to the surface normal and the direction [10] in the reciprocal surface net. E_v is the vacuum threshold, V_0 is the precalculated inner potential as referred to the vacuum level (cf. Fig. 3), E_s is the subthreshold predicted by a LEED calculation based on V_0, and E_{expt} is the observed subthreshold.

$h\,k$	θ (deg)	E_v (eV)	V_0 (eV)	E_s (eV)	E_{expt} (eV)	Feature
$10,\bar{1}1,0\bar{1}$						
$01,\bar{1}0,1\bar{1}$	0	30.8	−13.8	18.8	19.5	Large horizontal shoulder[a]
$\bar{2}1,\bar{1}\bar{1}$	5	80.0	−10.3	72.3	73.6	Peak[a]
$\bar{1}2,1\bar{2}$	5	93.0	−9.8		≈83	Inclined shoulder
$11,2\bar{1}$	5	108.3	−9.4		≈100	Horizontal shoulder
$\bar{2}0$	5	104.2	−9.5		≈100	Horizontal shoulder
$\bar{2}2,0\bar{2}$	5	113.7	−9.2	108	109	Small peak[a]
$02,2\bar{2}$	5	135.4	−8.7			
20	5	147.7	−8.5		136	Inclined shoulder

[a]Sharply localized, suitable for a determination of the inner potential.

we find two features of a similar origin at higher energies, the prominent peak at 73.6 eV and the small peak at 109 eV, which are localized sharply enough to be suitable for a determination of the inner potential. Fine-grid LEED calculations and comparison with the experimental data indicate that the precalculated inner potential $V_0(E)$ illustrated in Fig. 3 should be lifted by 0.7, 1.3, and 1 eV at the incidence energies 19.5, 73.6, and 109 eV, respectively, where prominent subthreshold effects are observed. The inner-potential values resulting from the three observations are plotted in Fig. 3. The errors given are ΔE from expression (10) and represent what we think is a possible accuracy in a determination of the inner potential from observations of subthresholds. The uncertainty in the angular setting of the incident beam is not taken into account by the error bars in Fig. 3.

A trial-and-error search of an inner potential from measured subthreshold effects will converge provided that the precalculated crystal potential describes the energy dependence of the electron scattering sufficiently well. Both the calculated inner potential and the phase shifts should be good approximations. For instance, we find that the theoretical spectra obtained from the $X\alpha$ potential[11] with $\alpha=0.4$ and 0.7 are not accurate enough to permit a determination of the energy dependence of the inner potential.

V. METRIC DISTANCE BETWEEN THEORY AND EXPERIMENT

Reproducibility is important in LEED work. The design of the so-called reliability indexes or R factors[13–15] arose from the need of an objective and efficient measure of the misfit between theory and experiment. Such a measure has to fulfill a few necessary conditions set by the LEED method. Since the configuration of atoms is imaged by constructive electron interference, the misfit measure must be sensitive to the position and shape of the peaks of the LEED spectra. Preferably, a misfit measure appropriate for structure determination should be insensitive to variations in spectra resulting from errors in nonstructural parameters having a slow energy variation: Debye temperature, interlayer attenuation (β and p_{abs}), and atomic scattering amplitude. In addition, the numerical data treatment should meet the standard requirement of being independent of the noise of the experimental recordings.

In the present work we separate the diffraction peaks and the slow energy variations by filtering the calculated and measured spectra. The method of metric distances suggested by Philip and Rundgren[12] will be used for measuring the misfit between the spectra thus obtained.

A. Filtering of spectra

The fast Fourier transform is conveniently used for separating the diffraction peaks from the slow energy variations. Let the spectrum $I_{hk}(E)$ of a beam hk be given in terms of N intensity values $f_0, f_1, \ldots, f_{N-1}$ distributed with a uniform mesh over the energy range E_1–E_2, and designate the Fourier components of the spectrum by $\phi_0, \phi_1, \ldots, \phi_{N-1}$. The Fourier transform and its inverse are

$$\phi_k = N^{-1/2} \sum_{j=0}^{N-1} f_j z^{jk} , \tag{11}$$

$$f_j = N^{-1/2} \sum_{k=0}^{N-1} \phi_k z^{-jk} , \tag{12}$$

where $z=\exp(2\pi i/N)$. If N is a power of 2, a special algorithm makes the computation particularly fast. One applies a high-pass Fourier filter to a spectrum by calculating the Fourier components from the original intensities f_j by expression (11), by setting a number of low-frequency components equal to zero, $\phi_n=\phi_{N-n}=0$, $n=1,2,\ldots$, and, finally, by calculating new intensities f_j from expression (12). The experimental and theoretical spectra of a beam hk are supposed to be processed with the same value of n.

For instance, in the present LEED study the 00 spectrum extends from $E_1=16$ eV to $E_2=190$ eV and the widths of the major peaks are of the order of 25 eV. The slow energy variations are represented by Fourier components having $n<7$. In this case, therefore, a few Fourier components can be neglected without loss of information about crystal geometry.

The notion of filtering is inherent in some of the current R factors. Zanazzi and Jona[13] differentiate the spectra twice in order to locate peaks by flanks having large slopes and by tops having large curvature. Pendry[15] differentiates the data once with a purpose to represent a LEED spectrum as a sum of Lorentzian peaks. A preprocessing of data by means of a Fourier filter can be made in the high-pass or low-pass mode depending on the structural or nonstructural parameters under consideration. Many types of filters exist, and the best choice depends on the LEED case under consideration. In the present work the Fourier filter is satisfactory since the calculated and measured spectra in Figs. 4–6 are very similar.

B. Metric distance between spectra

In this section we show that there exists a line of physical and mathematical arguments which most naturally lead to the use of metric distances for the comparison of theoretical and experimental spectra.[12]

1. Uncertainty of the experiment

We assume that the experimental spectra are recorded with an uncertainty that is negligible in relation to the changes which are possible in the theoretical spectra when different models of crystal structure are tested. The experimental spectra will therefore be considered as fixed.

2. Topological space of spectra

The space of spectra is generalized to a topological space. Topology introduces the notions of neighborhood and misfit. If, during a curve-fitting procedure, a theoretical spectrum f falls into a neighborhood given in advance of a fixed experimental spectrum g, one can say that f agrees with g with a measured misfit.

3. Convergence and uniqueness

Let us assume that $f^{(n)}$, $n=1,2,\ldots$, is a set of theoretical spectra corresponding to a sequence of choices of structural parameters. If for sufficiently high values of n, all $f^{(n)}$ are situated within a given neighborhood of the fixed spectrum g, one can say that the sequence $f^{(n)}$ converges towards g. For physical reasons it is necessary to stipulate that any trial sequence $f^{(n)}$ shall converge into a unique spectrum. This implies that a topological space of spectra has to be a Hausdorff space.[27]

4. Metric space of spectra

Metric spaces will be explored in this work. Though restricted in comparison with Hausdorff spaces, they can serve as frames for a great variety of curve-fitting procedures. A metric distance $D(f,g)$ between any pair of spectra f and g obeys the following metric axioms.[27]

(i) Strictness : $D(f,g)=0$, if, and only if, $f=g$.

(ii) Symmetry: $D(f,g)=D(g,f)$.

(iii) Triangle inequality: $D(f,g)\leq D(f,h)+D(h,g)$, where h is any third spectrum.

A set of spectra $f^{(n)}$ corresponding to successive choices of parameters, $n=1,2,\ldots$, is said to numerically converge provided $D(f^{(n)},g)<\epsilon$, where ϵ is a given tolerance. When $f^{(n)}$ and g are Fourier-filtered data, the result of $D(f^{(n)},g)<\epsilon$ is a convergence $f^{(n)}\rightarrow g$ modulo the Fourier components removed by the filter.

Explicit metrics will be considered in Sec. V C. In the spaces of spectra defined by the R factors of Zanazzi and Jona[13] and Pendry,[15] the strictness axiom (i) is not valid: It is, of course, true that f near g gives an R value near zero, but the converse does not necessarily hold. Therefore, it cannot be stated that these R factors satisfy the physical principle that convergence shall be unique. Curve fitting is currently made secure by the researcher's inspection of the various stages of the procedure, but if the researcher wishes to reduce the job of inspection, a metric distance is likely to be advantageous because of its uniqueness property.

5. Normalization

For a specified beam hk, the theoretical and experimental spectra are denoted by $f_{hk}(x)$ and $g_{hk}(x)$, where x signifies a normalized primary energy, $x=(E-E_1)/(E_2-E_1)$, or, as the case may be, a normalized incidence angle. It is already understood that we leave out the beam indices in contexts where a single beam is concerned. In cases where $f_{hk}(x)$ and $g_{hk}(x)$ are obtained on different intensity scales, the spectra are conveniently made commensurable by normalization to unity,[12–15]

$$\int_0^1 f_{kh}(x)dx=\int_0^1 g_{hk}(x)dx=1 \quad \text{for every } hk \ . \tag{13}$$

This normalization disregards the natural ratios between the intensities of the beams. In principle, the following normalization, $f_{hk}(x_0)=g_{hk}(x_0)$, applied to a single beam hk at a chosen energy x_0, suffices to establish a common theoretical and experimental intensity scale for all the beams. In this work we use expression (13).

6. Total metric

Given the metric distances $D(f_{hk},g_{hk})$ for the individual beams hk considered in a LEED investigation, a total metric associated with the collection of beams can be defined in the following way:

$$T^{(q)}=\left[\sum_{h,k} w_{hk}D(f_{hk},g_{hk})^q\right]^{1/q}, \quad w_{hk}>0, \quad \sum_{h,k} w_{hk}=1 \ , \tag{14}$$

where q is an integer greater than or equal to 1 and w_{hk} are relative weights on the beams. $T^{(q)}$ is a metric if $w_{hk}^{1/q}$ times $D(f_{hk},g_{hk})$ is a metric. This is certainly the case when w_{hk} is taken constant and independent of the intensities, for instance, proportional to the energy range where the experimental spectra g_{hk} are recorded. Zanazzi and Jona[13] use a total R factor that corresponds to $T^{(1)}$, and Pendry[15] uses another that corresponds to $T^{(2)}$. The total metrics defined in expression (14) are interrelated by the inequalities[12]

$$T^{(1)}\leq T^{(2)}\leq\cdots\leq T^{(\infty)}=\max_{h,k}\{D(f_{hk},g_{hk})\} \ . \tag{15}$$

C. Four metrics

The strong integrated distance D_1 is a standard metric used in x-ray crystallography and by many LEED workers,[13,14]

$$D_1(f,g)=\tfrac{1}{2}\int_0^1 |f(x)-g(x)|\,dx \ . \tag{16}$$

The metric D_1 reacts strongly by acquiring a large increment when peaks are moved out of place; this is the significance of the topological term strong[12,28] given to D_1.

Three weak distances which react by increments proportional to peak displacements will now be considered. They are expressed by means of the indefinite integrals

$$F(x)=\int_0^x f(t)dt \quad \text{and} \quad G(x)=\int_0^x g(t)dt \ . \tag{17}$$

With a normalized energy variable x and with normalized intensities $f(x)$ and $g(x)$, the functions $F(x)$ and $G(x)$ are confined to a square of unit edge where they increase monotonically from $F(0)=G(0)=0$ to $F(1)=G(1)=1$. In Fig. 9 we illustrate the integrated spectra by showing F and G for the 00 spectrum in Fig. 4.

We discuss the following.

(a) The weak integrated distance[12] $D_2(f,g)$,

$$D_2(f,g)=\int_0^1 |F(x)-G(x)|\,dx \ . \tag{18}$$

(b) The Levy distance (Refs. 12 and 29) $D_3(f,g)$. A line of slope -1 is moved across F and G, and for each position of the line, the segment between F and G is projected on the intensity axis. The longest projection is D_3.

(c) The Hausdorff distance (Refs. 12 and 30) $D_4(f,g)$. The distance is obtained by tracking F and G. At each point on the upper curve the shortest distance to the lower curve is measured and stored, and the process is repeated with "upper" and "lower" reversed. The longest distance stored is then D_4.

The strong metric D_1 and the weak metrics D_2, D_3, and D_4 take values that are less than or equal to 100%. This

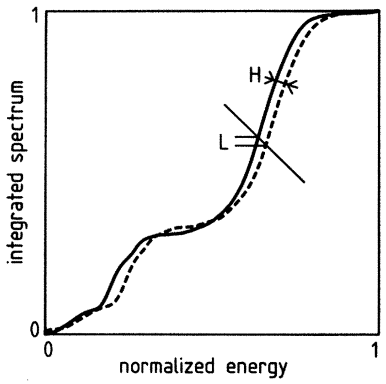

FIG. 9. Integrated spectra normalized to unit integral. Metric distances: D_2 denotes the area enclosed between the curves, D_3 denotes maximum vertical projection of the -1 slope segment L, and D_4 denotes maximum of the minimum distances H. Integral of the 00 spectrum in Fig. 4 is shown. Theoretical spectrum is intentionally displaced 5 eV.

follows from the confinement of the energy (angular) variable x to the interval (0,1) and from the normalization of the spectra to the unit integral. The limit 100% is attained for metric distances between the idealized spectra $\delta(x-a)$ and $\delta(x-b)$, where δ signifies Dirac's δ function and a and b denote points in the interval (0,1). As a matter of fact, the strong metric D_1 immediately becomes unity when $|a-b|$ differs the least from zero, whereas the weak metrics D_2, D_3, and D_4 grow linearly as $|a-b|$, which exceptionally becomes unity when one δ peak is situated at either end of the interval (0,1). As a rule of thumb one can say that D_1 less than 10% and D_2, D_3, and D_4 less than 1% indicate good agreement between two given spectra.

Numerically the four metrics have the following characteristics. Since they are based on the integration of data, they are perfectly stable with respect to noise, whereas the R factors[13,15] use differentiation of the data and require smoothing. The four metrics give rise to very fast algorithms, and calculation times are considerably shorter than for the R factors.[13,15]

C. Linear response to variations of structural parameters

The weak metrics give a linear response to small variations of an intensity curve. As a consequence, in every case where the beam intensities vary linearly with respect to small variations of a structural parameter, the metric distances will likewise respond linearly to that parameter. This is the physical basis for the use of weak metric distances for structural analysis.

Taking f and g to be a theoretical and an experimental spectrum, we shall study the response of the metric distances, $D_i(f,g)$, $i=2,3,4$, to a variation of f to $f+\Delta f$. Because of the strictness axiom (Sec. V B) the response of $D(f,g)$ to Δf is never zero unless $\Delta f=0$, and because of the triangle inequality

$$|D(f+\Delta f,g)-D(f,g)| \le D(f,f+\Delta f) , \tag{19}$$

the response is limited by $\Delta D=D(f,f+\Delta f)$. We shall therefore take ΔD as an approximate value of the response of $D(f,g)$ to the variation Δf for any spectrum g.

Changes of the position and of the height of peaks are of particular interest in diffraction theory. As a matter of illustration we shall consider a spectrum f which contains a narrow peak, $H\delta(x-x_0)$, situated at the point x_0 and having the area H. A displacement Δx and an area increment ΔH of the peak under consideration give a varied spectrum $f+\Delta f$ that contains a peak $H\delta(x-x_0-\Delta x)$ or a peak $(H+\Delta H)\delta(x-x_0)$. In Ref. 12 and an accompanying report[31] it was shown that the responses to the changes Δx and ΔH are

$$\frac{\Delta D_2}{\Delta x}=H \quad \text{and} \quad \frac{\Delta D_3}{\Delta x}=\frac{\Delta D_4}{\Delta x}=1 \tag{20}$$

and

$$\frac{\Delta D_2}{\Delta H}=\int_0^{x_0} F(x)dx+\int_{x_0}^1 [1-F(x)]dx ,$$
$$\frac{\Delta D_3}{\Delta H} \quad \text{and} \quad \frac{\Delta D_4}{\Delta H} \le \max[F(x_0),1-F(x_0)] . \tag{21}$$

The response to ΔH depends on the position x_0 of the peak and on the shape of the integrated spectrum F. In particular, in applications where F varies in the neighborhood of $F(x)=x$, the values of $\Delta D_i/\Delta H$ are of the order of $\frac{1}{2}$.

The integrals F and G consist of a succession of rounded-off steps corresponding to the peaks of the spectra f and g. If f and g have the same long-range behavior, F and G have many crossovers or run close together with vertical separations less than the average height of the steps. Under these circumstances the weak metrics are sensitive to the position and shape of peaks. If f and g exhibit slow energy variations which are substantially different, F and G bend apart much more than the average step height, and the weak metrics lose sensitivity to short-range features.

High-pass filtering is one possibility of enhancing the diffraction peaks of f and g (Sec. V A). There are also metrics which are less sensitive to slow-energy variation than D_2, D_3, and D_4, though a metric will always give some response to any misfit because of the strictness axiom. For instance, the metric

$$D_{2y}(f,g)=\min_y \left\{ \int_0^1 |F(x)+y-G(x)|\,dx \right\} \tag{22}$$

brings $F(x)$ and $G(x)$ together by a constant shift y, so that $D_{2y}(f,g) \le D_2(f,g)$. New metrics D_{3y} and D_{4y} are derived in a similar way by minimization of D_3 and D_4 with respect to a constant shift of $F(x)$ relative to $G(x)$.

D. Application to the copper (111) surface

Theoretical and experimental spectra for the three beams 00, 10, and 01 are compared by means of the strong metric D_1 and the weak metrics D_{2y}, D_{3y}, and D_{4y}. The total metric $T^{(q)}$ for the set of beams is calculated from expression (14) with weights w_{hk} proportional to the con-

sidered energy ranges 16—190, 48—190, and 31—190 eV for the 00, 10, and 01 beams. We take $q=1$ so that the total metric is the linear average of the beam metrics (see Table II). We exclude a part of the 10 spectrum corresponding to the experimentally difficult region just above 30.8 eV where the 10 beam emerges grazingly in the vacuum with a very high intensity. We likewise exclude a part of the 01 spectrum where the beam propagates through a node of the differential cross section and the calculated spectrum is inaccurate (Sec. IV A). Afterwards we apply the total metric to the disconnected pieces of the 01 spectrum.

The comparison of theoretical and experimental spectra in Table II is made for a grid of overlayer relaxations $\Delta d=0.005$ Å about the bulk interlayer spacing $d=2.084$ Å and for a grid of shifts ΔV_0 of the inner potential $V_0(E)$. Our study of the subthreshold effect in Sec. IV B indicates that the precalculated $V_0(E)$, given a constant shift ΔV_0, agrees closely with the measurements. Each value of Δd demands a complete LEED calculation with $V_0(E)$ fixed, whereas ΔV_0 is easily added during the calculation of the metric distances. In the 2D space of Δd and ΔV_0, each metric distance is mapped by isometric contours which prove similar to ellipses. They are centered about a minimum point, the Δd and ΔV_0 values of which indicate the best fit to experiment as established by the metric under consideration. The strong metric D_1 is applied directly to the spectra and gives an upper bound for the misfit of theory and experiment. The weak metrics D_{2y}, D_{3y}, and D_{4y} are applied after the spectra have been processed through a Fourier high-pass filter with $n=1$ in the manner defined by expressions (11) and (12). The filtering of spectra detaches the diffraction features from a slowly varying nonstructural background which is somewhat different for the calculation and the measurement.

Table II shows that the spread of Δd and ΔV_0 over four metrics and over three beams is small, although the Δd and ΔV_0 values for the 10 beam differ noticeably from the values given by the total metric. Filtering helps significantly to diminish the spread for the weak metrics. The total metric distances listed at the bottom of Table II give $\Delta V_0=1.3\pm0.3$ eV. The result follows essentially from a matching of the Bragg peaks which predominate over the subthreshold effects in the metric analysis. The agreement with the energy-dependent ΔV_0 determined separately from the subthreshold effects observed in the 00 beam (Sec. IV B) is satisfactory.

Figure 10 illustrates the total metric distances as functions of Δd for the pertaining optimum values of ΔV_0. The metric distance against relaxation curves prove to have their minima placed in close agreement, and the surface relaxation Δd is found to be $(-0.7\pm0.5)\%$ of the interlayer separation in the bulk. The error given is estimated from the spread of $\delta V_0=0.3$ eV in the metric determination of V_0 by the simple argument that LEED measures layer separation in units of the inverse wave number $k=(E-V_0)^{1/2}$. Hence, the relative error in the layer separation is at least

$$d^{-1}\delta d=-k^{-1}\delta k=\tfrac{1}{2}(E-V_0)^{-1}\delta V_0\ .$$

Since the 00 spectrum has an important low-energy peak which greatly influences the metric distances, we take $E-V_0$ equal to 30 eV and find $d^{-1}\delta d=0.5\%$ as written above.

VI. DISCUSSION AND CONCLUSIONS

A. New method of determining the inner potential

In a structure determination by LEED, the inner potential has to be known as a function of energy, $V_0(E)$, in particular, below 100 eV where the energy variation is rapid. In principle, a LEED calculation of the major peaks of the spectra of several beams determines both the crystal structure and $V_0(E)$, but in practice one is met with the difficult problem of separating the geometrical parameters and the function $V_0(E)$. The difficulty has hitherto been circumvented in two ways. Either the structure determination is performed at such high energies (above 100 eV) that the inner potential can be considered constant,[5] or else a function $V_0(E)$ is supplied by a purportedly reliable electron-gas theory.[10,11]

Another possibility to determine fixed points on the function $V_0(E)$ arises if the LEED spectra exhibit pronounced subthreshold effects. Since an excited scattering

TABLE II. Surface relaxation Δd, inner-potential correction ΔV_0, and metric distance D calculated from the 00, 10, and 01 intensity spectra. Δd signifies surface minus bulk interlayer spacing, ΔV_0 is a constant shift of $V_0(E)$, and 1, 2y, 3y, and 4y stand for the metrics D_1, D_{2y}, D_{3y}, and D_{4y} and the corresponding totals.

	Δd (%)				ΔV_0 (eV)				D (%)			
Beam	1	2y	3y	4y	1	2y	3y	4y	1	2y	3y	4y
00[a]	−0.7	−0.5	−0.7	−0.5	1.0	1.1	1.2	1.5	7	0.30	0.54	0.59
10[b]	−0.3	0	0	0	2.2	2.5	2.7	2.7	8	0.47	0.84	0.93
01[c]	−0.5	−0.6	−0.8	−0.7	1.7	1.2	1.2	1.5	6	0.32	0.52	0.60
Total	−0.7	−0.6	−0.8	−0.7	1.1	1.6	1.2	1.5	8	0.39	0.76	0.82

[a]Energy range 16—190 eV.
[b]Energy range 48—190 eV.
[c]Energy range 31—190 eV with 96—124 eV excluded.

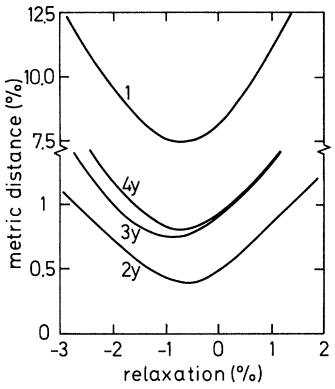

FIG. 10. Surface relaxation determined by means of metric distances. The strong distance D_1 is applied directly to the calculated and measured spectra; the weak distances D_{2y}, D_{3y}, and D_{4y} are applied after Fourier high-pass filtering. Minima indicate a relaxation of -0.7%.

channel pseudoparallel to the surface extends over several layers below the surface, a subthreshold effect has a linewidth of the order of 2 eV. Because of the small linewidth, a subthreshold effect will determine a point on the energy-dependent inner potential with an accuracy superior to what is attainable from the positions of the major peaks. We believe that a calculated subthreshold effect fitted to a measured one could settle a point on $V_0(E)$ within a tolerance of ± 0.1 eV, if the Rydberg fine structure at the beam emergences in vacuum[22] are used for calibrating the energy scale. Moreover, in this kind of determination the value of $V_0(E)$ is not coupled to the value of the interlayer spacing d at the surface. (We speak of a crystal composed of identical layers.) Once $V_0(E)$ is known, the surface relaxation and related parameters can be determined accurately from the Bragg peaks.

In a recent LEED investigation on the (110) surface of nickel by Gauthier *et al.*,[32] the energy-dependent inner potential is determined from the major peaks of intensity against energy spectra by means of reliability indexes[13,15] applied to a very large data base (beam spectra over totally 3000 eV). The inner potential found for nickel shows a similar variation with energy as the one determined for copper in the present work from a calculated potential and three measured subthreshold effects (Fig. 3); the difference is less than 1 eV over the common energy range 30—120 eV. The agreement is satisfactory owing to both metals having similar electron density.

The method of using, first, subthreshold effects for establishing the inner potential and, afterwards, the Bragg structures for determining surface geometry, has, in our view, a great promise. The energy-dependent inner potential derived from the theory of the excited electron gas can be checked in a direct manner against LEED measurements. A local excited-state potential can then be used for interpolating between the fixed points $V_0(E)$ supplied by the experiment. When the inner potential is a quantitatively well-known function of energy, structure determination by LEED will be accurate also at very low energies.

B. Determination of geometrical structure

When looking at a calculated and a measured LEED spectrum, one intuitively pays attention to diffraction peaks (the eye is a filter) and evaluates their agreement (the eye is a misfit measurer). The visual inspection concentrating on Bragg peaks is simulated by means of high-pass filters and metric distances. For methodological reasons we prefer to use metric distances and filters for measuring the misfit between theory and experiment, rather than the reliability indexes used in many LEED investigations today. Our approach implies that the filtering and the misfit measurement can be designed, tested, and applied separately. The presently used reliability indexes have filter and misfit measure in implicit combinations. The metric distances work with integrated data and are intrinsically stable with respect to noise. In contradistinction, the reliability indexes defined on differentiated spectra require careful smoothing of data before they are applied.

Weak metric distances are used for comparing theoretical and experimental LEED spectra because of their linear response to small intensity variations. For physical reasons, then, the weak metric distances also give a linear response to variations of structural parameters. The structural result of this paper is that the topmost interlayer spacing at the (111) surface of copper is contracted by $(0.7\pm 0.5)\%$ from the bulk value. The comparison of theory and experiment is made by metric distances between spectra and Fourier-type high-pass filtering of spectra. The four metrics which we use determine the surface relaxation with a very small spread (Table II).

At the 50th anniversary of the discovery of electron diffraction it was estimated[33] that LEED was capable of measuring interatomic distances with 0.1-Å accuracy. The prediction is now radically improved to 0.01 Å in LEED situations, where the subthreshold effect and the Rydberg fine structure can be used for establishing the energy-dependent inner potential $V_0(E)$. This sets up a very accurate wave-number standard $[E-V_0(E)]^{1/2}$ not only for LEED but for all kinds of electron spectroscopies for surfaces.

ACKNOWLEDGMENTS

Discussions with R. Baudoing, C. Gaubert, and Y. Gauthier on many aspects of this work have been of particular value. This work was supported in part by the Swedish National Research Council.

[1]S. Å. Lindgren, L. Walldén, J. Rundgren, and P. Westrin, Phys. Rev. Lett. 50, 368 (1983).
[2]J. Rundgren and G. Malmström, Phys. Rev. Lett. 38, 836 (1977); A. Adnot and J. D. Carette, *ibid.* 38, 1084 (1977).
[3]L. R. Bedell and H. E. Farnsworth, Surf. Sci. 41, 165 (1974).
[4]R. C. Jaklevic and L. C. Davis, Phys. Rev. B 26, 5391 (1982).
[5]S. P. Tear, K. Röll, and M. Prutton, J. Phys. C 14, 3297 (1981).
[6]P. O. Gartland and B. J. Slagsvold, Phys. Rev. B 12, 4047 (1975).
[7]P. Heimann, J. Hermanson, H. Miosga, and H. Neddermeyer, Phys. Rev. B 20, 3059 (1979).
[8]D. Westphal, D. Spanjaard, and A. Goldman, J. Phys. C 13, 1361 (1959).
[9]L. Hedin and B. I. Lundqvist, J. Phys. C 4, 2064 (1971).
[10]J. Neve, J. Rundgren, and P. Westrin, J. Phys. C 15, 4391 (1982).
[11]J. Neve, P. Westrin, and J. Rundgren, J. Phys. C 16, 1291 (1983).
[12]J. Philip and J. Rundgren, in *Proceedings of the Conference on Determination of Surface Structure by LEED, Yorktown Heights, 1980,* edited by P. M. Marcus and F. Jona (Plenum, New York, 1983).
[13]E. Zanazzi and F. Jona, Surf. Sci. 62, 61 (1977).
[14]M. A. van Hove, S. Y. Tong, and M. H. Elconin, Surf. Sci. 64, 85 (1977).
[15]J. B. Pendry, J. Phys. C 13, 937 (1980).
[16]W. J. Tegart, *The Electrolytic and Chemical Polishing of Metals* (Pergamon, London, 1959).
[17]J. B. Pendry, *Low Energy Electron Diffraction* (Academic, London, 1974).
[18]J. Rundgren and A. Salwén, Comput. Phys. Commun. 7, 369 (1974); 9, 312 (1975); J. Phys. C 9, 3701 (1976).
[19]M. A. van Hove and S. Y. Tong, *Surface Crystallography by LEED* (Springer, Berlin, 1979).
[20]D. J. Titterington and C. G. Kinniburgh, Comput. Phys. Commun. 20, 237 (1980).
[21]L. I. Schiff, *Quantum Mechanics,* 3rd ed. (McGraw-Hill, New York, 1968), p. 130.
[22]G. Malmström and J. Rundgren, J. Phys. C 13, L61 (1980); J. M. Baribeau and J. D. Carette, Phys. Rev. B 23, 6201 (1981).
[23]M. Rasolt and H. L. Davis, Phys. Rev. B 20, 5059 (1979).
[24]*International Tables for X-ray Crystallography* (Kynoch, Birmingham, England, 1969), Vol. 1.
[25]G. Malmström and J. Rundgren, Comput. Phys. Commun. 19, 263 (1980).
[26]F. H. Herbstein, Adv. Phys. 10, 313 (1961).
[27]E. M. Patterson, *Topology* (Oliver and Boyd, Edinburgh, Scotland, 1956).
[28]A. E. Taylor, *Functional Analysis* (Wiley, New York, 1958), p. 151.
[29]B. V. Gnedenko and A. N. Kolmogorov, *Limit Distributions for Sums of Independent Random Variables* (Addison-Wesley, Cambridge, Mass., 1954), p. 32.
[30]J. L. Kelley, *General Topology* (Van Nostrand, New York, 1955), p. 131.
[31]J. Philip and J. Rundgren, Royal Institute of Technology Report TRITA-MAT No. 35, 1980.
[32]Y. Gauthier, R. Baudoing, and L. Clarke, J. Phys. C. 15, 3231 (1982).
[33]J. B. Pendry, in *Electron Diffraction 1927—1977,* edited by P. J. Dobson, J. B. Pendry, and C. J. Humphreys (Institute of Physics, Bristol, England, 1978), pp. 205—217.